Polynuclear Manganese(II) Complexes with Robson-type Ligands. Synthesis, Characterization, Molecular Structure, and Magnetic Properties†

Dominique Luneau, Jean-Michel Savariault, Patrick Cassoux, and Jean-Pierre Tuchagues*
Laboratoire de Chimie de Coordination du CNRS, Unité No 8241 liée par convention à l'Université Paul Sabatier, 205 route de Narbonne, 31077 Toulouse Cedex, France

The synthesis, infrared and e.s.r. spectra, and variable-temperature magnetic susceptibility of seven manganese(II) complexes with macrocyclic Robson-type ligands and chloride, bromide, or acetate and perchlorate anions are described. The ligands include a symmetric macrocycle (L^1) resulting from the condensation of 2,6-diformyl-4-methylphenol with 1,3-diaminopropane and asymmetric macrocycles resulting from the two-step condensation of 2,6-diformyl-4-methylphenol with 1,3-diaminopropane and 1,3-diamino-2-hydroxypropane (L^2). The crystal molecular structure of $[Mn_2L^2(MeCO_2)]ClO_4$ has been established by *X*-ray diffraction methods. This complex crystallizes in the triclinic system, space group $P\bar{1}$, in a cell of dimensions $a = 12.513(8)$, $b = 13.67(1)$, $c = 8.699(8)$ Å, with $Z = 2$. The structure was solved by the direct method and refined by a succession of difference Fourier syntheses and least-squares refinements. An unresolved disorder of the perchlorate anion has set the agreement indices of the structure to $R = 0.114$ and $R' = 0.142$ for 2 968 reflections. *X*-Ray powder patterns and a large angle *X*-ray scattering study allowed us to determine the main structural features of the six remaining complexes. Minor changes, either in the macrocyclic ligand or in the nature of the anions, result in different molecular structures and magnetic behaviour of the complexes. The complexes $[Mn_2L^1Cl_2]$, $[Mn_2L^2Cl_2]$, $[Mn_2L^1Br_2]$, and $[Mn_2L^2Br_2]$ are built from isolated binuclear units with an axially-distorted square-pyramidal geometry around each manganese ion. The manganese ion is displaced out of the macrocyclic ligand plane towards the apical halide anion. The high-spin manganese(II) ions exhibit a very weak intramolecular ferromagnetic exchange interaction ($J = +0.1$ to $+0.3$ cm^{-1}) in all four complexes. $[Mn_2L^1(MeCO_2)]ClO_4$ and $[Mn_2L^2(MeCO_2)]ClO_4$ include binuclear units bridged by acetate anions into infinite chains. The manganese ions are displaced out of the macrocyclic ligand plane towards the acetato oxygen atom and the co-ordination geometry is essentially square pyramidal. The high-spin manganese(II) ions exhibit a weak intramolecular antiferromagnetic exchange interaction ($J = -0.8$ cm^{-1}) in both complexes. The extended intermolecular interaction mediated by the acetato groups between the manganese ions of a chain is very weak but still reflected by the powder e.s.r. spectra. $[Mn_2L^3]ClO_4$ is most probably built from tetranuclear species including two binuclear units bridged through their alcoholate anions. The high-spin manganese(II) ions of this complex are involved in intramolecular antiferromagnetic exchange interactions stronger than those usually reported for manganese(II). $[Mn_2L^1(MeCO_2)]ClO_4$, $[Mn_2L^2(MeCO_2)]ClO_4$, and $([Mn_2L^3]ClO_4)_2$ are the first antiferromagnetically exchange-coupled manganese(II) complexes including Robson-type ligands.

Coupled metal centres play an important role in both natural and synthetic catalysts. Several metallo-enzymes such as cytochrome oxidase, nitrogenase, and the photosynthetic water oxidation site include coupled metal centres and catalyse important reactions under mild conditions.

Our previous contributions to the understanding of the magnetic exchange interactions present in such systems have focused on neutral manganese complexes containing linear polydentate ligands with nitrogen and oxygen donors.[1,2] The first example of a macrocyclic ligand able to enclose two metal centres was reported by Pilkington and Robson[3] [L^1, Figure 1(*a*)]. Homobinuclear complexes of the $[M_2L^1Cl_2]$ series (M = Cu^{II}, Ni^{II}, Co^{II}, Fe^{II}, or Mn^{II}) have been prepared and investigated in order to study their structural features and magnetic properties.[3–6] In these binuclear complexes, each

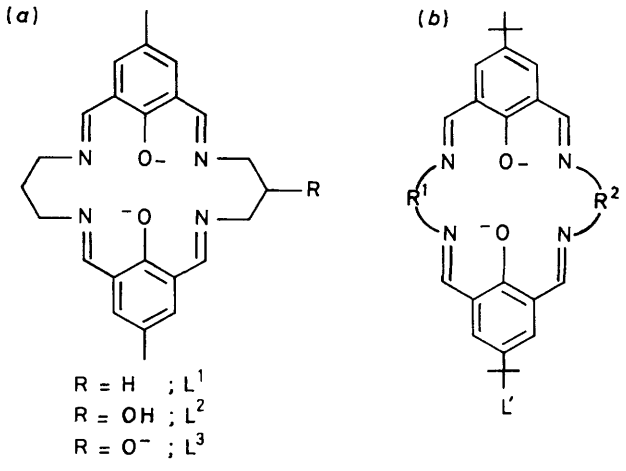

Figure 1. Schematic representation of the ligands R^1, $R^2 = (CH_2)_3$, $CH_2CMe_2CH_2$, $(CH_2)_4$, or 2,2'-biphenylene; see ref. 12 for combinations

† *Supplementary data available* (No. SUP 56703, 18 pp.): magnetic susceptibility data, e.s.r. spectral data, *X*-ray powder diffraction data. See Instructions for Authors, *J. Chem. Soc., Dalton Trans.*, 1988, Issue 1, pp. xvii—xx.

Non-S.I. units employed: G = 10^{-4} T, c.g.s. unit = $10^6/4\pi \times$ S.I.

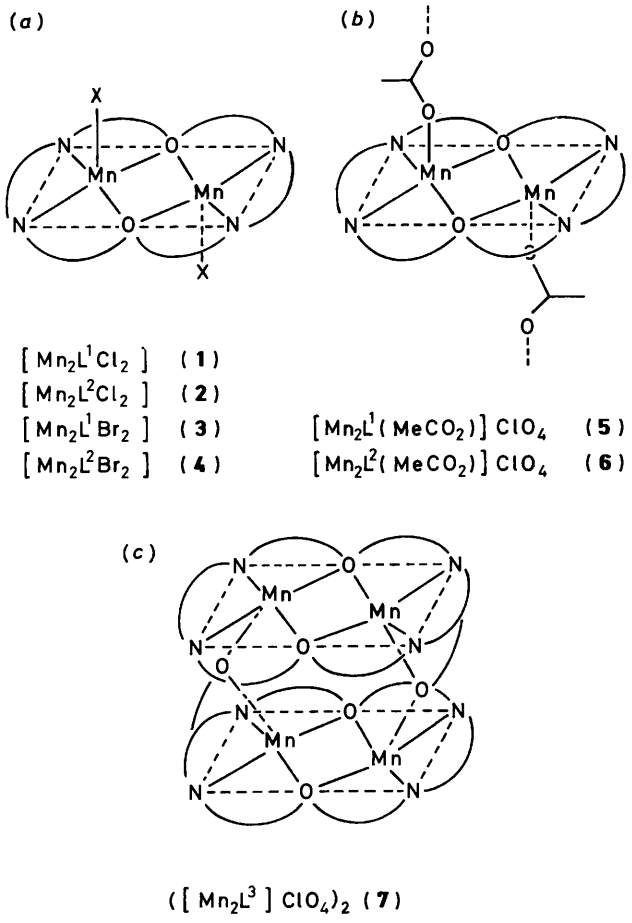

Figure 2. Schematic representation, abbreviation, and numbering of the complexes studied

metal ion is five-co-ordinate with an essentially square-pyramidal co-ordination geometry.[4,5] The decrease in net antiferromagnetic exchange interaction along the series $[M_2L^1Cl_2]$ from Cu^{II} to Fe^{II}, and the appearance of a net ferromagnetic interaction in the manganese complex, were attributed to an increasing number of unpaired electrons and an increasing metal-to-ligand-plane distance on going from copper to manganese.[6] Similar studies and conclusions have been obtained for heterobinuclear complexes of the series $[CuML^1Cl_2]$, where M is Ni^{II}, Co^{II}, Fe^{II}, or Mn^{II}.[7,8] The exchange parameter follows the same trend across the $[M_2L^1(py)_4][BF_4]_2$ series[9] (M = Ni^{II}, Co^{II}, or Fe^{II}) where the metal ions are six-co-ordinate with an octahedral co-ordination geometry. Again, it was concluded that this variation probably reflects the increasing number of unpaired electrons in going from one complex to another.

The ligand L^1 and related macrocyclic binucleating ligands L′ [Figure 1(*b*)] have been used to prepare new mixed-valence complexes.[10–12] The *X*-ray molecular structure determination of $[Co^{II}Co^{III}L^1Br_2(MeOH)_2][Br_3]$ and $[Cu^{II}Cu^{I}L^1(MeOH)_{0.5}]ClO_4$ shows localized valence states in the solid state for these two mixed-valence complexes.[10,11c] Both photoassisted and thermal intramolecular electron transfers have been observed in solution for $[Cu^{II}Cu^{I}L^1(MeOH)_{0.5}]ClO_4$ and related $[Cu^{II}Cu^{I}L']BF_4$ complexes, involving either symmetrical or asymmetrical Robson-type ligands, L′.[11,12]

This survey of the results afforded when using such binucleating macrocycles with different axial ligands to tune the magnetic exchange interaction between two metal centres shows the significance of such studies in the understanding of (*i*) magnetic exchange interactions mediated by superexchange pathways, and (*ii*) intramolecular electron transfer in mixed-valence systems. This survey also shows the lack of experimental results for manganese complexes involving Robson-type ligands, which is surprising considering the relevance of such complexes to the manganese site for water oxidation in photosynthesis, involving two pairs of magnetically coupled manganese centres.[13]

These observations prompted us to perform the synthesis and physico-chemical study of manganese(II) complexes with Robson-type ligands with the aim of (*i*) evaluating the variations of the intramolecular magnetic exchange interaction between manganese(II) ions when the superexchange pathway is modified by changes in either the binucleating macrocycle or the metal-to-ligand-plane distance afforded by different apical ligands; (*ii*) achieving electrochemical and/or chemical oxidations to manganese(II)–manganese(III) species.

In this paper we report the synthesis and i.r., e.s.r., and variable-temperature magnetic susceptibility results for seven manganese(II) complexes involving either the symmetric Robson ligand L^1, or the related asymmetric ligands, L^2 and L^3 [Figure 1(*a*)], and either chloride, bromide, perchlorate, or acetate and perchlorate anions. *X*-Ray structural studies including *X*-ray crystal structure determination, *X*-ray powder patterns, and large angle *X*-ray scattering allow a better understanding of the magnetic properties of these complexes. Figure 2 gives a schematic representation of the postulated or determined geometries.

Experimental

Materials.—1,3-Diamino-2-hydroxypropane (Fluka) was sublimed prior to use. 1,3-Diaminopropane was purchased from Fluka in high purity grade and used as received. 2,6-Diformyl-4-methylphenol was prepared according to literature methods.[7,14] All other chemicals were reagent grade or equivalent. Toluene was refluxed over sodium–benzophenone and distilled under argon. Dimethylformamide (dmf) was shaken over KOH for 1 h, refluxed over BaO for 30 min and distilled under argon. The centre cut (10—90%) was further distilled under vacuum. All solvents were degassed under vacuum prior to use.

Preparation of the Complexes.—$[Mn_2L^1Cl_2]$ (**1**), $[Mn_2L^1Br_2]$ (**3**), *and* $[Mn_2L^1(MeCO_2)]ClO_4$ (**5**). These complexes were prepared according to the procedure reported previously for $[Mn_2L^1Cl_2]$.[3]

$[Mn_2L^2Cl_2]$ (**2**), $[Mn_2L^2Br_2]$ (**4**), *and* $[Mn_2L^2(MeCO_2)]ClO_4$ (**6**). These complexes have been obtained through an *in situ* multi-step reaction similar to that described by Long and Hendrickson.[12]

$[Mn_2L^3]ClO_4$ (**7**). The complex $[Mn_2L^2(MeCO_2)]ClO_4$ (**6**) (5 mmol) was dissolved in dry deoxygenated methanol (30 cm^3). To the resulting solution, sodium methanolate (10 mmol) dissolved in deoxygenated methanol (10 cm^3) was added dropwise with stirring. The resulting yellow precipitate was filtered, washed with deoxygenated methanol (2 × 20 cm^3) and dried under vacuum for 6 h.

As an added precaution, all complexes were prepared in Schlenk glassware, under a purified nitrogen atmosphere. The complexes were directly transferred and stored in an inert-atmosphere box (Vacuum Atmospheres H. E. 43-2) equipped with a dry train (Jahan EVAC 7). The analytical results for the complexes are in good agreement with the theoretical values for C, H, N, halide and Mn (Table 1).

Physical Measurements.—Elemental analyses were carried out at the Laboratoire de Chimie de Coordination microanalyti-

Table 1. Analytical data for manganese(II) complexes

Compound	Analysis (%) C	H	N	Mn	Halide
(1) $[Mn_2L^1Cl_2]$·MeOH	49.85 (48.80)	4.90 (4.85)	9.40 (9.10)	17.80 (17.85)	12.15 (11.55)
(2) $[Mn_2L^2Cl_2]$·MeOH	48.30 (47.55)	4.45 (4.75)	8.55 (8.85)	16.85 (17.40)	11.55 (11.25)
(3) $[Mn_2L^1Br_2]$·MeOH	43.40 (42.60)	4.50 (4.25)	7.70 (7.95)	14.60 (15.60)	21.50 (22.70)
(4) $[Mn_2L^2Br_2]$·MeOH	41.45 (41.70)	3.75 (4.15)	7.45 (7.80)	15.00 (15.25)	20.80 (22.20)
(5) $[Mn_2L^1(MeCO_2)]ClO_4$·MeOH	46.85 (46.15)	4.30 (4.70)	8.00 (7.95)	15.85 (15.65)	5.05 (5.05)
(6) $[Mn_2L^2(MeCO_2)]ClO_4$·MeOH	45.50 (45.10)	4.30 (4.60)	7.85 (7.80)	14.90 (15.30)	5.05 (4.95)
(7) $[Mn_2L^3]ClO_4$·MeOH	45.75 (45.55)	4.40 (4.40)	8.30 (8.50)	16.55 (16.70)	4.45 (5.40)

Table 2. Summary of crystal and intensity collection data

Formula	$C_{26}H_{29}ClMn_2N_4O_9$
M	686.9
Crystal system	triclinic
a/Å	12.513(8)
b/Å	13.67(1)
c/Å	8.699(8)
α/°	100.50(8)
β/°	90.54(7)
γ/°	92.43(7)
U/Å^3	1 461.5
Z	2
$F(000)$	740
D_m/g cm^{-3}	1.56(3) (measured by flotation in C_6H_5Br–CCl_4)
D_c/g cm^{-3}	1.560
Space group	$P\bar{1}$
Radiation	Mo-K_α (graphite monochromator)
λ/Å	0.710 69
Linear absorption coefficient (cm^{-1})	9.49
T/°C	20
Receiving aperture (mm)	5.0 × 4.0
Take-off angle (°)	3.5
Scan mode	ω–2θ
Scan range (°)	1.10 + 0.35 tan θ
2θ limits (°)	63

cal laboratory in Toulouse for C, H, and N, and at the Service Central de Microanalyses du CNRS in Vernaison for the other elements. I.r. spectra were recorded on a Perkin-Elmer 983 spectrophotometer coupled with a Perkin-Elmer infrared data station. Samples were run as CsBr pellets prepared under nitrogen in the dry-box.

Variable-temperature magnetic susceptibility data were obtained on polycrystalline samples with a Faraday-type magnetometer equipped with a continuous flow Oxford Instruments cryostat. Magnetic field strengths between 4 and 6 kG were employed. The independence of the magnetic susceptibility from magnetic fields up to 12 kG was checked over the whole temperature range. Mercury tetrakis(thiocyanato)cobaltate was used as a susceptibility standard. The absolute accuracy of the temperature was ±0.2 K. The relative accuracy of the apparent weight increase when the magnetic field is applied was significantly better than 1%. Diamagnetic corrections were applied using Pascal's constants. Least-squares computer fittings of the magnetic susceptibility data were carried out with an adapted version of the function-minimization program, STEPT.[15]

E.s.r. spectra were obtained on a Bruker 200 TT spectrometer equipped as previously described.[2] Solution and powdered samples were loaded in 3-mm (X-band) or 1-mm (Q-band) cylindrical quartz tubes in the dry-box and subsequently degassed and sealed under vacuum.

The X-ray diffraction powder patterns were obtained with a Guinier powder diffractograph (Cu-K_α radiation wavelength 1.5418 Å) for the seven complexes described in this study.

X-Ray Crystal Structure Determination of $[Mn_2L^2(MeCO_2)]ClO_4$ (**6**).—Crystals of complex (**6**) were obtained by slow interdiffusion of solutions of the mononuclear complex $[ML^2(MeCO_2)_2]$ and of the manganese(II) perchlorate salt in methanol. The crystals were free of methanol solvate molecules. The crystals belong to the triclinic system, space group $P\bar{1}$. The selected crystal was an orange-yellow parallelepiped of approximate dimensions 0.48 × 0.29 × 0.15 mm. It was glued onto a glass fibre and mounted on an Enraf-Nonius CAD4 diffractometer. Cell constants were obtained from a least-squares fit of 25 reflections. Crystal and intensity collection data are summarized in Table 2. A total of 9 258 reflections were recorded, to a 2θ(Mo) maximum of 63°, by procedures described elsewhere.[16] Intensity standards, recorded periodically, showed no significant variation during measurements. Reflections were corrected for Lorentz and polarization effects,[17] 2 968 of which with $I > \sigma(I)$ were used in subsequent calculations. No absorption corrections were made.

Structure Solution and Refinement.—The starting point of the structure was determined by using the direct method.[18] A succession of difference Fourier syntheses and least-squares refinements revealed the positions of all non-hydrogen atoms. During structure determination it appeared that the perchlorate anion was disordered over two chlorine and six oxygen positions. Several unsuccessful attempts, including a rigid body of tetrahedral symmetry per chlorine, were made to find a model that could be refined, taking into account the aforementioned statistical disorder. A similar situation is often encountered for ClO_4 and BF_4.[19,20] As the interest in this structure does not lie in the geometry of the perchlorate anion these attempts were not pursued further. All atoms except those of the perchlorate moiety were refined anisotropically. Due to the unresolved perchlorate disorder, the last difference Fourier synthesis did not allow location of the hydrogen atoms.

The atomic scattering factors used were those proposed by Cromer and Waber[21] with anomalous dispersion effects.[22] The final full-matrix least-squares refinement, minimizing $\Sigma w(|F_o| - |F_c|)^2$, converged to $R = \Sigma||F_o| - |F_c||/\Sigma|F_o| = 0.114$ and $R' = [\Sigma w(|F_o| - |F_c|)^2/\Sigma w|F_o|^2]^{\frac{1}{2}} = 0.142$ with a weighting scheme of $w = 0.75/[\sigma^2(F) + 0.008F^2]$. The goodness of fit was $S = 1.05$ with 2 968 observations and 375 variables. All calculations were performed on a VAX 11/730 DEC computer using the programs SDP,[17] SHELX 76,[23] MULTAN,[18] and ORTEP.[24] The two independent binuclear units of $[Mn_2L^2(MeCO_2)]ClO_4$ are shown in Figure 3 with the atom numbering. Final fractional atomic co-ordinates with their estimated standard deviations are given in Table 3.

Additional material available from the Cambridge Crystallographic Data Centre comprises thermal parameters.

Large Angle X-Ray Scattering Studies.—A powered sample of complex (**7**) was carefully ground and pressed (400 kg cm^{-2}) into a 0.9-mm thick pellet and mounted on a goniometer head. The diffuse spectrum scattered by the sample irradiated with graphite-monochromatized Mo-K_α radiation (λ = 0.710 69 Å)

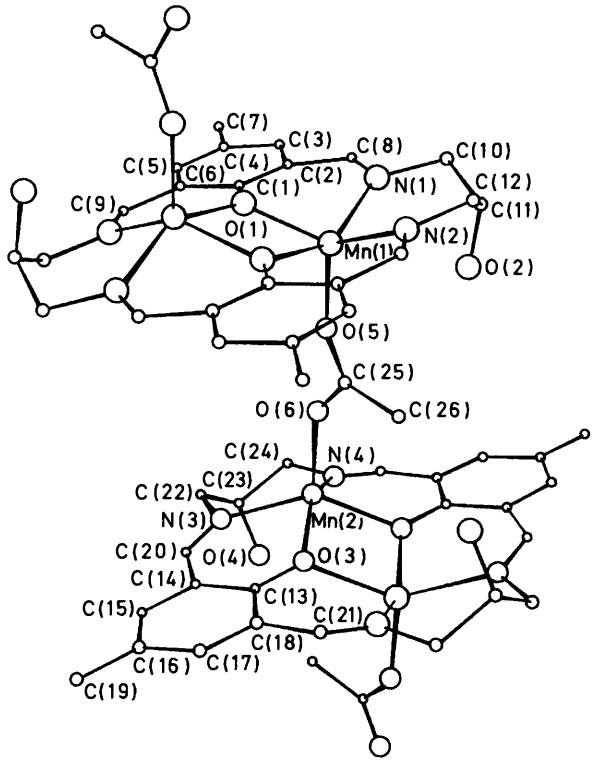

Figure 3. ORTEP view of the $[Mn_2L^2(MeCO_2)]^+$ cation chain

was obtained using an ω–σ goniometer equipped with a linear position-sensitive detector.[25,26] The pellet was orientated perpendicularly to the *X*-ray beam when the goniometer angles equalled zero. Scattered intensities were measured with the θ–2θ scan mode. Some 2 000 equidistant points were measured in 20 h with $1.5 < 2\theta < 66°$.

The data processing was carried out on the aforementioned VAX 11/730 DEC computer using the LASIP system.[26] The scattered intensities were corrected for polarization and absorption effects, normalized by comparison with the sum of coherent and incoherent independent intensities using the methods of Krogh-Moe, and Burian *et al.*[27] The atomic scattering factors for the Mn, Cl, O, N, and C atoms were taken from ref. 21, and Compton diffusion factors from ref. 28.

The experimental radial distribution function, $F(r)$, which shows the distribution of the interatomic distances in complex (7), was obtained using the Zernicke and Prins relation.[29] The theoretical radial distribution function, $F(r)$, was calculated for structural models by the Fourier transform of Debye's formula of theoretical intensities.[30]

Results and Discussion

The experimental results indicate that the seven complexes studied in this paper are divided into three geometry types. As shown in Figure 2, $[Mn_2L^1Cl_2]$ (**1**), $[Mn_2L^2Cl_2]$ (**2**), $[Mn_2L^1Br_2]$ (**3**), and $[Mn_2L^2Br_2]$ (**4**) have two equivalent manganese(II) ions experiencing a distorted square-pyramidal co-ordination geometry with one halide anion bonded to each manganese ion in an axial site [Figure 2(*a*)]. Complexes $[Mn_2L^1(MeCO_2)]ClO_4$ (**5**) and $[Mn_2L^2(MeCO_2)]ClO_4$ (**6**) consist of binuclear units bridged by acetato groups to afford infinite chains. In these chains the manganese(II) ions experience square-pyramidal co-ordination geometries with one oxygen atom of the bridging acetato group bonded to each manganese ion in an axial site [Figure 2(*b*)]. We postulate a tetranuclear structure for $[Mn_2L^3]ClO_4$ (**7**): the co-ordination of the alcoholate function of the L^3 ligands of two adjacent binuclear units to one of the manganese ions of the partner binuclear unit affords the type of structure shown in Figure 2(*c*).

Table 3. Fractional atomic co-ordinates of non-hydrogen atoms for $[Mn_2L^2(MeCO_2)]ClO_4$ with estimated standard deviations in parentheses

Atom	*X*/*a*	*Y*/*b*	*Z*/*c*
Mn(1)	0.394 2(1)	0.065 8(1)	0.000 9(2)
N(1)	0.324 4(8)	0.083 9(7)	−0.220(1)
N(2)	0.245 0(8)	0.003 3(8)	0.080(1)
O(1)	0.533 7(6)	0.028 3(6)	−0.133 2(9)
O(2)	0.198(2)	0.187(2)	0.009(3)
C(1)	0.566 5(9)	0.065 8(7)	−0.254(1)
C(2)	0.497 4(9)	0.105 6(8)	−0.352(1)
C(3)	0.533(1)	0.142(1)	−0.484(1)
C(4)	0.645(1)	0.143 8(9)	−0.521(1)
C(5)	0.715(1)	0.106 4(9)	−0.417(1)
C(6)	0.679 8(9)	0.067 1(8)	−0.294(1)
C(7)	0.685(1)	0.182(1)	−0.669(1)
C(8)	0.380(1)	0.105 5(9)	−0.333(1)
C(9)	0.764 1(9)	0.036(1)	−0.204(1)
C(10)	0.204(1)	0.084(1)	−0.241(2)
C(11)	0.150(1)	0.106(1)	−0.083(2)
C(12)	0.139(1)	0.016(1)	0.003(2)
Mn(2)	0.573 3(2)	0.480 8(1)	0.342 8(2)
N(3)	0.581 1(8)	0.593 2(7)	0.195(1)
N(4)	0.746 1(8)	0.482 4(7)	0.375(1)
O(3)	0.432 2(6)	0.550 3(6)	0.430 0(8)
O(4)	0.762(2)	0.686(2)	0.345(2)
C(13)	0.360(1)	0.586 8(9)	0.346(1)
C(14)	0.391(1)	0.630 7(8)	0.216(1)
C(15)	0.316(1)	0.671 1(9)	0.130(1)
C(16)	0.205(1)	0.666(1)	0.167(2)
C(17)	0.179(1)	0.624(1)	0.294(2)
C(18)	0.251(1)	0.580 5(9)	0.383(1)
C(19)	0.125(1)	0.711(1)	0.071(2)
C(20)	0.503(1)	0.642(1)	0.165(1)
C(21)	0.204(1)	0.545 1(9)	0.514(1)
C(22)	0.682(1)	0.609(1)	0.110(2)
C(23)	0.782(1)	0.620(1)	0.213(2)
C(24)	0.816(1)	0.519(1)	0.252(2)
C(25)	0.444(1)	0.282(1)	0.200(1)
C(26)	0.354(1)	0.301(1)	0.313(2)
O(5)	0.449 0(8)	0.204 2(6)	0.105(1)
O(6)	0.516 8(7)	0.352 2(6)	0.203 2(8)
Cl(1)	0.034 4(7)	0.201 7(8)	0.409(1)
Cl(2)	0.030(1)	0.247(1)	0.353(2)
O(7)	0.137(2)	0.171(2)	0.392(2)
O(8)	0.051(2)	0.318(2)	0.467(3)
O(9)	−0.037(4)	0.132(4)	0.340(7)
O(10)	0.040(5)	0.305(5)	0.275(8)
O(11)	0.003(3)	0.190(3)	0.535(5)
O(12)	−0.027(3)	0.196(4)	0.254(5)

Analytical Results and Infrared Spectroscopy.—On the basis of elemental analysis data (Table 1), the complexes prepared by using either L^1 or L^2 and equimolar quantities of manganese(II) acetate and manganese(II) chloride or bromide have the formula $[Mn_2L^1X_2]$·MeOH and $[Mn_2L^2X_2]$·MeOH, respectively (X = Cl or Br). The complexes prepared from either L^1 or L^2 and equimolar ratios of manganese(II) acetate and manganese(II) perchlorate have the formula $[Mn_2L^1(MeCO_2)]ClO_4$·MeOH and $[Mn_2L^2(MeCO_2)]ClO_4$·MeOH, respectively. The complex prepared by deprotonating the ligand alcoholic function of $[Mn_2L^2(MeCO_2)]ClO_4$ has the unit formula $[Mn_2L^3]ClO_4$·MeOH.

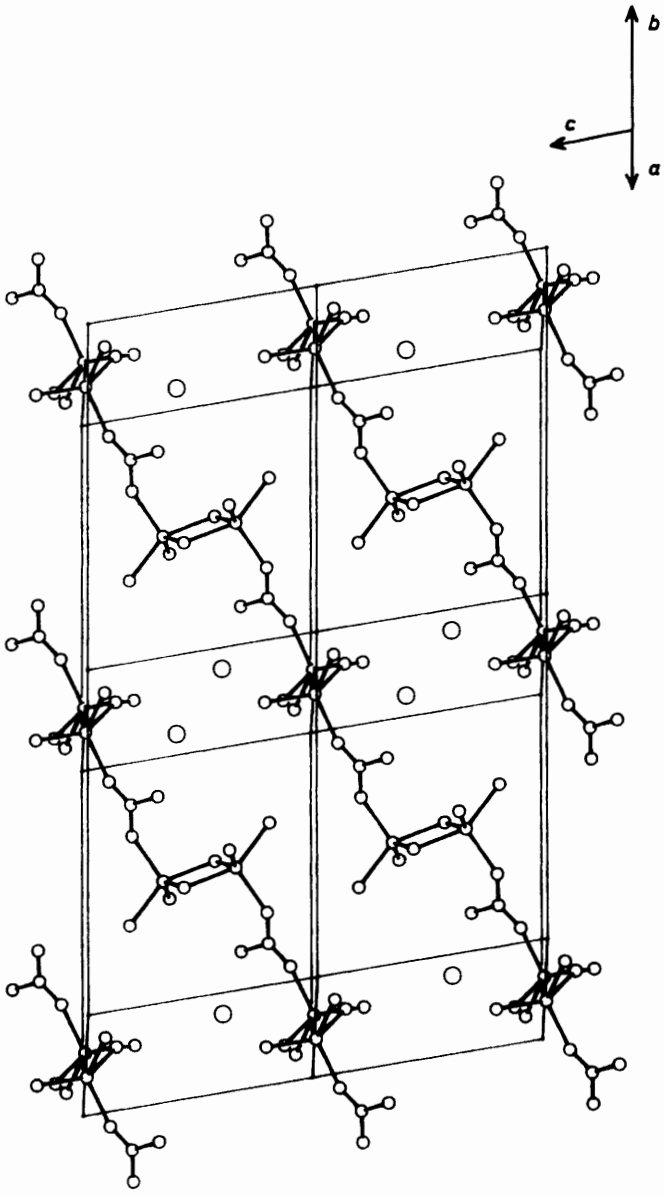

Figure 4. ORTEP view of four unit cells of $[Mn_2L^2(MeCO_2)]ClO_4$ (**6**)

The infrared spectra of the four complexes incorporating halide anions (**1**)—(**4**) are virtually indistinguishable, as already stated for the complexes of L^1 previously described.[3,7,9,11b] The i.r. spectra of the three complexes incorporating perchlorate anions (**5**)—(**7**) exhibit two additional absorptions (1 090 and 620 cm^{-1}) characteristic of unco-ordinated perchlorate.[3,9] The two complexes incorporating an acetate anion, (**5**) and (**6**), exhibit three more bands (1 580, 1 445, and 1 420 cm^{-1}) characteristic of a bridging acetato group.[31] Considering the structural information obtained for the parent complexes involving L^1 and various metal ions,[4,5,9] together with their i.r. characterization,[3,7,9,11b] it can be already postulated that the Mn^{II} ions of the seven complexes studied herein experience three different ligand environments: the manganese(II) ions of the complexes (**1**)—(**4**) have a N_2O_2X donor set (X = Cl or Br); those of the complexes (**5**) and (**6**) have a N_2O_3 donor set, including an acetato bridge; and the unit formula of $[Mn_2L^3]ClO_4$ includes two equivalent manganese(II) ions having N_2O_3 or N_2O_4 donor sets, depending on whether a methanol solvate molecule is co-ordinated or not.

Molecular Structure of $[Mn_2L^2(MeCO_2)]ClO_4$ (**6**).—The perspective view of the cation in Figure 3 shows two independent binuclear units bridged by an acetato group affording infinite chains along [011]. These chains are stacked in planes parallel to the (100) plane. The disordered perchlorate anions are located between these planes. The detailed view of the cation chains depicted in Figure 4 shows that the main planes of two adjacent binuclear units are nearly parallel (5.4°). Bond lengths and angles are given in Table 4.

The angle between the directions defined by the planes O(5), Mn(1), Mn(1′), and O(6), Mn(2), Mn(2′) of two adjacent units is 61.1°, due to the zig-zag conformation of the chains. Between the chains the shortest Mn(1)–Mn(2) and Mn(1)–Mn(1) distances are 7.35 and 8.70 Å, respectively. Two adjacent chains overlap partially through a benzene ring of one chain [associated with Mn(1)] and two benzene rings [Mn(1) and Mn(2), respectively] of the second chain. The average distances between the benzene ring [Mn(1)] of the first chain and the benzene rings [Mn(1) and Mn(2)] of the second chain are 3.6 and 3.8 Å respectively.

In the chain, the macrocyclic ligands of two adjacent binuclear units have different conformations: the 2-hydroxypropane bridge located between N(1) and N(2) is directed towards the oxygen atom O(5) of the acetato ligand while the corresponding bridge located between N(3) and N(4) is directed away from the oxygen atom O(6) of the same acetato ligand. The O(2) atom is statistically shared by C(11) and C(11′). Similarly, O(4) is statistically shared by C(23) and C(23′). Considering the distances between O(2) and O(10) (3.29 Å) on the one hand, and O(4) and O(7) (2.95 Å) or O(8) (2.85 Å) on the other [O(7), O(8), and O(10) pertain to the ClO_4 anion], it is clear that the hypothesis of a hydrogen bonding network between the ClO_4 anion and both O(2) and O(4) oxygen atoms can not be excluded. This would afford two types of ClO_4 anions equally distributed among the hydrogen atoms bonded to O(2) and O(4) and those not having O(2) and O(4) in their environment. It is interesting to note that such a distribution could account not only for the statistical distribution of O(2) among C(11) and C(11′) and O(4) among C(23) and C(23′), but also for the disorder of the ClO_4 anion.

In both binuclear units, the manganese environment is square pyramidal with two nitrogen and two oxygen atoms from the macrocyclic ligand in the base plane and an oxygen atom from an acetate anion in the apical position. The manganese cation is 0.61 Å above the base plane, towards the acetate ligand. Two pyramids share an O ··· O edge to form a centrosymmetric binuclear unit with an average Mn–Mn separation of 3.27 Å. The interatomic distance between the Mn(1) and Mn(2) atoms separated by the acetate moiety is 6.22 Å. The out of plane position of the manganese ions may be due not only to the relative sizes of the manganese(II) cation and macrocyclic ligand cavity, but also to the opposite trends imposed by the acetate bite on one hand and the benzene-ring stacking interactions previously mentioned on the other.

X-Ray Powder Diffraction Spectra.—The complexes containing chloride [(**1**) and (**2**)] and bromide [(**3**) and (**4**)] anions have very similar *X*-ray powder diffraction spectra indicating approximately the same unit cell. Comparison of their spectra with the spectrum of $[Co_2L^1Br_2]$ calculated[32] from the fractional atomic co-ordinates of this complex[4] allowed us to index the four spectra (see SUP 56703) and propose cell parameters (Table 5) similar to those published for $[Co_2L^1Br_2]$.[4] Comparison of the observed line intensities for complexes (**3**) and (**4**) with those calculated for $[Co_2L^1Br_2]$

Table 4. Bond lengths (Å) and angles (°) for $[Mn_2L^2(MeCO_2)]ClO_4$ (**6**) with estimated standard deviations in parentheses. Prime indicates atoms related by the inversion centre

Mn environment			
Mn(1)–O(1)	2.14(1)	Mn(2)–O(3)	2.12(1)
Mn(1)–O(1′)	2.100(4)	Mn(2)–O(3′)	2.097(3)
Mn(1)–O(5)	2.03(5)	Mn(2)–O(6)	2.041(3)
Mn(1)–N(1)	2.16(1)	Mn(2)–N(3)	2.17(1)
Mn(1)–N(2)	2.19(5)	Mn(2)–N(4)	2.18(1)
O(1)–Mn(1)–O(1)	79.3(3)	O(3)–Mn(2)–O(3)	77.8(3)
O(1)–Mn(1)–O(5)	96.3(3)	O(3)–Mn(2)–O(6)	103.5(4)
O(1)–Mn(1)–N(1)	84.4(3)	O(3)–Mn(2)–N(3)	84.8(3)
O(1)–Mn(1)–N(2)	143.3(3)	O(3)–Mn(2)–N(4)	144.0(3)
O(1′)–Mn(1)–O(5)	103.7(3)	O(3′)–Mn(2)–O(6)	104.5(4)
O(1′)–Mn(1)–N(1)	148.0(3)	O(3′)–Mn(2)–N(3)	147.5(3)
O(1′)–Mn(1)–N(2)	83.8(3)	O(3′)–Mn(2)–N(4)	84.8(3)
O(5)–Mn(1)–N(1)	105.4(4)	O(6)–Mn(2)–N(3)	106.2(3)
O(5)–Mn(1)–N(2)	119.4(4)	O(6)–Mn(2)–N(4)	111.5(3)
N(1)–Mn(1)–N(2)	93.4(3)	N(3)–Mn(2)–N(4)	93.7(4)
Ligand environment			
O(1)–C(1)	1.31(1)	O(3)–C(13)	1.32(2)
O(2)–C(11)	1.36(3)	O(4)–C(23)	1.36(2)
N(1)–C(8)	1.28(2)	N(3)–C(20)	1.25(2)
N(1)–C(10)	1.51(2)	N(3)–C(22)	1.50(1)
N(2)–C(9′)	1.29(2)	N(4)–C(21′)	1.27(1)
N(2)–C(12)	1.51(2)	N(4)–C(24)	1.53(1)
C(1)–C(2)	1.41(2)	C(13)–C(14)	1.42(2)
C(1)–C(6)	1.46(1)	C(13)–C(18)	1.41(2)
C(2)–C(3)	1.40(2)	C(14)–C(15)	1.36(2)
C(2)–C(8)	1.48(2)	C(14)–C(20)	1.49(2)
C(3)–C(4)	1.45(2)	C(15)–C(16)	1.43(2)
C(4)–C(5)	1.43(2)	C(16)–C(17)	1.37(2)
C(4)–C(7)	1.56(2)	C(16)–C(19)	1.52(3)
C(5)–C(6)	1.36(2)	C(17)–C(18)	1.40(2)
C(6)–C(9)	1.43(2)	C(18)–C(21)	1.44(2)
C(10)–C(11)	1.52(2)	C(22)–C(23)	1.52(2)
C(11)–C(12)	1.55(3)	C(23)–C(24)	1.56(3)
O(5)–C(25)	1.23(2)	C(25)–C(26)	1.51(2)
O(6)–C(25)	1.29(2)		
O(1)–C(1)–C(2)	123(1)	O(3)–C(13)–C(18)	120(1)
O(1)–C(1)–C(6)	121(1)	O(3)–C(13)–C(14)	121(1)
C(8)–N(1)–C(10)	116(1)	C(20)–N(3)–C(22)	116(1)
C(9′)–N(2)–C(12)	114(1)	C(21′)–N(4)–C(24)	115(1)
C(2)–C(1)–C(6)	116(1)	C(14)–C(13)–C(18)	119(1)
C(1)–C(2)–C(3)	123(1)	C(13)–C(14)–C(15)	121(1)
C(1)–C(2)–C(8)	123(1)	C(13)–C(14)–C(20)	124(1)
C(3)–C(2)–C(8)	114(1)	C(15)–C(14)–C(20)	114(1)
C(2)–C(3)–C(4)	120(1)	C(14)–C(15)–C(16)	120(1)
C(3)–C(4)–C(7)	121(1)	C(15)–C(16)–C(17)	117(1)
C(3)–C(4)–C(5)	117(1)	C(15)–C(16)–C(19)	119(1)
C(5)–C(4)–C(7)	123(1)	C(17)–C(16)–C(19)	124(1)
C(4)–C(5)–C(6)	123(1)	C(16)–C(17)–C(18)	125(1)
C(1)–C(6)–C(5)	122(1)	C(13)–C(18)–C(21)	128(1)
C(1)–C(6)–C(9)	125(1)	C(17)–C(18)–C(2)	114(1)
C(5)–C(6)–C(9)	113(1)	N(3)–C(20)–C(14)	127(1)
N(1)–C(8)–C(2)	129(1)	N(4)–C(21)–C(18)	126(1)
N(2′)–C(9)–C(6)	127(1)	N(4)–C(22)–C(23)	114(1)
N(1)–C(10)–C(11)	111(1)	O(4)–C(23)–C(22)	107(1)
O(2)–C(11)–C(10)	111(1)	O(4)–C(23)–C(24)	111(1)
O(2)–C(11)–C(12)	111(1)	C(22)–C(23)–C(24)	113(1)
C(10)–C(11)–C(12)	115(1)	C(13)–C(18)–C(17)	117(1)
N(2)–C(12)–C(11)	109(1)	N(4)–C(24)–C(23)	113(1)
O(5)–C(25)–O(6)	120(1)	O(6)–C(25)–C(26)	117(1)
O(5)–C(25)–C(26)	122(1)		
Perchlorate			
Cl(1)–O(7)	1.37(2)	Cl(1)–O(12)	1.54(5)
Cl(1)–O(8)	1.59(3)	Cl(2)–O(8)	1.28(3)
Cl(1)–O(9)	1.33(5)	Cl(2)–O(12)	1.21(5)
Cl(1)–O(11)	1.21(5)		

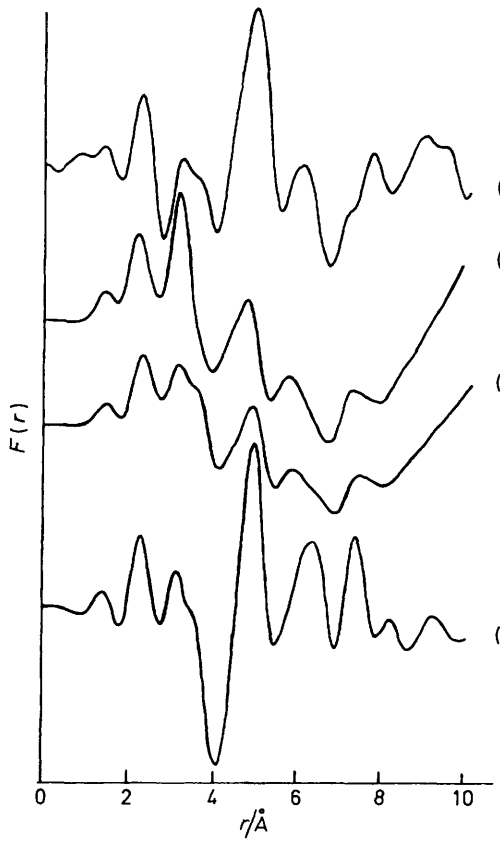

Figure 5. Radial distribution function (r.d.f.) for $([Mn_2L^3]ClO_4)_2$ (**7**): (*a*) experimental; (*b*) simulated for a Mn_2L^3 binuclear unit as described for (**6**) in the molecular structure section; (*c*) simulated for a modified Mn_2L^3 binuclear unit as described in the large angle *X*-ray scattering investigation section; (*d*) simulated for a tetranuclear complex built from two Mn_2L^3 binuclear units as depicted in (*c*)

indicates that these complexes are probably isostructural with $[Co_2L^1Br_2]$. The line intensities for complexes (**1**) and (**2**) are not like those of $[Co_2L^1Br_2]$. However, considering the $Z = 2$ multiplicity of (**1**) and (**2**), and the similarity of the spectra of complexes (**1**)—(**4**), this does not rule out isomorphism between (**1**) and (**2**), and $[Co_2L^1Br_2]$. The substitution of both bromide anions for chloride anions implies substantial changes in the reflection intensities.

Complexes (**5**) and (**6**), containing acetate bridges, crystallize with different unit cells: the *X*-ray powder diffraction spectra of these complexes are very different from one another and from those of complexes (**1**)—(**4**). Complex (**6**) exhibits an experimental *X*-ray diffraction powder spectrum similar to that calculated[32] from the molecular crystal structure described in the previous section. The experimental *X*-ray diffraction powder spectrum of complex (**5**) has been tentatively indexed (SUP 56703) according to the trial and error method TREOR.[33] Based upon the *X*-ray crystal structure determination of complex (**6**) two triclinic cells can be proposed (Table 6). The first proposed unit cell has a multiplicity of $Z = 2$ and a volume approximately equal to that of complex (**6**). The *a*, *b*, α, β, and γ cell parameters are similar to those obtained for complex (**6**). The *c* cell parameter is 2.66 Å larger than that of complex (**6**). This lengthening of *c* may be understood as an increase of the interchain distance in the plane (100) possibly resulting from the presence of a methanol solvent molecule in the structure of complex (**5**). The second proposed unit cell has a multiplicity of $Z = 1$ and a volume approximately half that of complex (**6**).

Table 5. Cell parameters for $[Co_2L^1Br_2]$, $[Mn_2L^1Br_2]$, $[Mn_2L^2Br_2]$, $[Mn_2L^1Cl_2]$, and $[Mn_2L^2Cl_2]$

Compound	a/Å	b/Å	c/Å	β/°	U/Å^3	Z	D_m/g cm^{-3}	D_c/g cm^{-3}
$[Co_2L^1Br_2]$[a]	9.872 3(5)	16.891(1)	8.074 5(5)	102.06(1)	1 316.73	2	1.79(3)	1.796
$[Mn_2L^1Br_2]$[b]	9.8(7)	17.07(9)	8.29(5)	102.6(5)	1 352.32	2	1.72(3)	1.727
$[Mn_2L^2Br_2]$[b]	9.80(9)	16.9(1)	8.21(6)	102.1(7)	1 334.61	2	1.70(3)	1.711
$[Mn_2L^1Cl_2]$[b]	10.05(3)	17.30(5)	8.17(3)	101.4(3)	1 391.78	2	1.52(3)	1.543
$[Mn_2L^2Cl_2]$[b]	9.95(5)	17.27(6)	8.09(6)	102.1(5)	1 359.52	2	1.51(3)	1.462

[a] Calculated from the *X*-ray crystal structure determination of $[Co_2L^1Br_2]$ (ref. 4). [b] Calculated from the refined *X*-ray powder diffraction pattern by using the TREOR program.[33]

Table 6. Cell parameters for $[Mn_2L^2(MeCO_2)]ClO_4$ and $[Mn_2L^1(MeCO_2)]ClO_4$

Compound		a/Å	b/Å	c/Å	α/°	β/°	γ/°	U/Å^3	Z	D_m/g cm^{-3}	D_c/g cm^{-3}
$[Mn_2L^2(MeCO_2)]ClO_4$[a]		12.513(8)	13.67(1)	8.699(8)	100.50(8)	90.54(7)	92.43(7)	1 461.5	2	1.56(3)	1.56
$[Mn_2L^1(MeCO_2)]ClO_4$[b]	1	11.85(2)	13.21(3)	11.40(2)	110.8(2)	94.2(2)	110.7(2)	1 518.3	2	1.53(3)	1.54
	2	8.81(2)	11.38(1)	8.76(2)	94.4(2)	114.9(1)	83.3(2)	791.9	1	1.53(3)	1.47

[a] Calculated from the *X*-ray crystal structure determination of $[Mn_2L^2(MeCO_2)]ClO_4$. [b] Calculated from the refined *X*-ray diffraction powder pattern by using the TREOR program.[33]

The second interpretation supposes that the conformation of the binuclear unit of complex (**5**) is unique contrarily to the existence of two different conformations of the binuclear units observed for (**6**). Unlike (**6**) complex (**5**) does not have any alcoholic oxygen atom in the propane-1,3-diyl unit bridging the imine nitrogen atoms. This implies that both propane units of each macrocyclic ligand are equivalent in (**5**). The disorder of the central carbon atom of the corresponding propane units reported for iron,[9] cobalt,[4] and copper[5] complexes of the same macrocycle supports the hypothesis of a unique binuclear unit conformation. A non-centred triclinic system results from this interpretation: the acetato bridges are directed along the *a* axis, thus preventing the existence of any centre of symmetry.

Complex (**7**), which exhibits no diffraction pattern, is an amorphous material and is discussed in the following section.

Large Angle X-Ray Scattering Investigation of Complex (**7**).—Elemental analysis and i.r. spectroscopy indicate that the basic unit of complex (**7**) is Mn_2L^3 with a non-co-ordinating ClO_4 anion. Consequently, a single Mn_2L^3 unit can be used as a first stage for fitting the experimental radial distribution function (r.d.f.) shown in Figure 5(*a*). With this purpose, we used the structure of a binuclear unit of (**6**) determined by *X*-ray diffraction as a model for (**7**). As shown in Figure 5(*b*), the resulting calculated co-ordination peak has its maximum at 2.2, instead of 2.3 Å in the experimental r.d.f. curve, Figure 5(*a*). The calculated r.d.f. curve in Figure 5(*b*) exhibits a maximum at 3.2 Å corresponding to both the manganese–manganese and manganese–20 nearest carbon atoms separations. However, the 3.2 Å range in the experimental r.d.f. curve is characterized by a 3.2—3.6 Å split peak. Both the shift of the co-ordination peak to higher *r* values and the splitting of the 3.2 Å peak suggest a larger manganese–ligand plane separation than that assumed in the first model based on the *X*-ray molecular structure of the cation of (**6**). An increase in the manganese–ligand plane distance will result both in a larger metal–metal separation and a larger metal-to-ligand mean distance. Consequently, for the second simulation we assumed a single Mn_2L^3 unit with a larger metal-to-ligand plane distance. From over 20 simulations the best fit for both the co-ordination peak and the 3.2—3.6 Å range was obtained for a 0.82 Å metal-to-ligand plane distance associated with a 0.2 Å increase in the distance between the projections of the manganese atoms onto the ligand plane [Figure 5(*c*)]. With respect to the description of the molecular structure of (**6**), this series of simulations was carried out assuming one of two possibilities: (*a*) the alcoholate oxygen atom of the macrocyclic ligand is directed towards the nearest manganese atom in the binuclear unit; (*b*) the alcoholate oxygen atom is directed in the opposite direction. It is of interest to note that the best fit in this series [Figure 5(*c*)] was obtained assuming hypothesis (*a*).

The most important feature of the experimental r.d.f. curve [Figure 5(*a*)] is a very intense peak at 4.9 Å. However, all simulated r.d.f. curves already mentioned [Figure 5(*b*) and (*c*)] exhibit weak and broad features in this 4.9 Å range. Such a large difference in intensity indicates that important intermolecular interactions are operating at this distance in complex (**7**). Two types of hypothesis can be made in order to account for these interactions: (*i*) a chain built up from the co-ordination of the alcoholate oxygen atom pertaining to a given binuclear unit as pictured in Figure 6(*a*); (*ii*) a tetranuclear complex built up from the binding of two binuclear units through the co-ordination of the alcoholate oxygen atom of each binuclear unit to a manganese atom of the second binuclear unit as pictured in Figure 6(*b*). A large number of simulations based on the 'chain model,' (*i*), including single-and multi-chain hypotheses (up to four chains) with different positions and orientations did not afford a good fit of the experimental r.d.f. curve.

Finally, from over 80 simulations a reasonable fit was obtained [Figure 5(*d*)] by assuming the hypothesis of a tetranuclear complex, (*ii*), including two binuclear units as described above [hypothesis (*a*)] interacting as pictured in Figure 6(*b*). The main structural features of this final tetranuclear model are: intra binuclear Mn–Mn distance, 3.6 Å; inter binuclear Mn–Mn distances, 4.6, 4.9, and 6.1 Å; Mn–in-plane ligands average distance, 2.3 Å; Mn–O (alcoholate) inter-binuclear distance, 3.1 Å; Mn–O (alcoholate) intra-binuclear distance 3.6 Å. The poor agreement observed at distances higher than 6 Å presumably results from the fact that we did not take into account interactions between neighbouring tetranuclear complexes. We also ignored the presence of the ClO_4 anions.

Magnetic Susceptibility.—The magnetic susceptibility data at 280, 50, and 5 K for complexes (**1**)—(**7**) are summarized in Table 7. The detailed data are available as supplementary material (SUP 56703) except for complex (**1**) for which our data agree perfectly well with those mentioned and fitted in a previous study.[6] The effective magnetic moment per manganese(II) ion, $\mu_{eff.}$(Mn) increases appreciably as the temperature is decreased below *ca.* 50 K for complexes (**1**)—(**4**), indicating that a weak

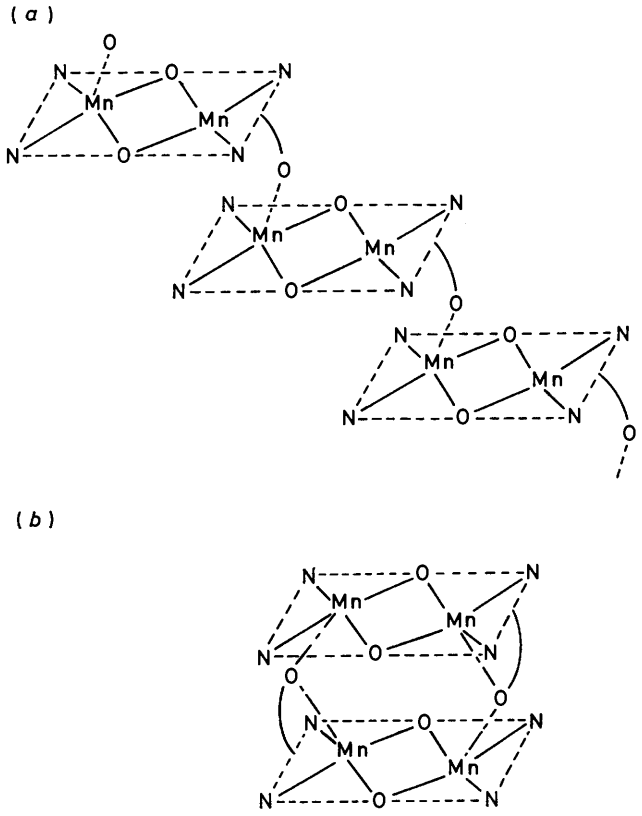

Figure 6. Schematic drawing of; (*a*) a possible single chain; (*b*) two interacting binuclear units resulting in the tetranuclear model affording the best fit

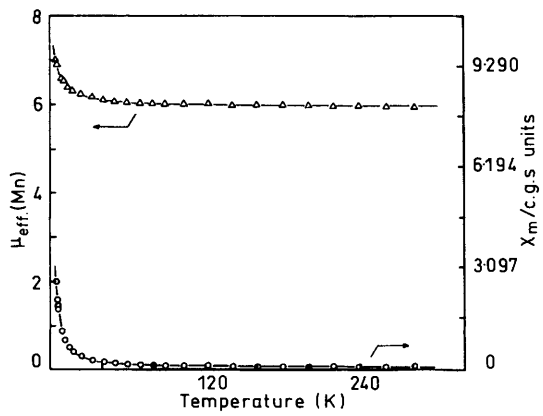

Figure 7. Variable-temperature magnetic susceptibility data for $[Mn_2L^2Cl_2]$ (**2**). The solid lines result from a least-squares fit of the data to the theoretical equation for isotropic magnetic exchange in a binuclear unit with $S_1 = S_2 = \frac{5}{2}$

ferromagnetic exchange interaction is present in all four complexes. The data for $[Mn_2L^2Cl_2]$ (**2**) are illustrated in Figure 7.

On the other hand for complexes (**5**) and (**6**), the effective magnetic moment per manganese(II) ion decreases greatly as the temperature is decreased below *ca.* 50 K, indicating that an antiferromagnetic exchange interaction is present in both complexes. The data for $[Mn_2L^1(MeCO_2)]ClO_4$ (**5**) are illustrated in Figure 8. The *X*-ray crystal structure determination of (**6**) indicates that the binuclear units are bridged by

Table 7. Effective magnetic moments, $\mu_{eff.}$(Mn)

	Compound	280 K	50 K	5 K
(1)	$[Mn_2L^1Cl_2]$	5.89	6.00	6.80
(2)	$[Mn_2L^2Cl_2]$	5.92	6.10	6.87
(3)	$[Mn_2L^1Br_2]$	6.11	6.15	6.96
(4)	$[Mn_2L^2Br_2]$	6.22	6.30	7.18
(5)	$[Mn_2L^1(MeCO_2)]ClO_4$	5.85	5.40	2.85
(6)	$[Mn_2L^2(MeCO_2)]ClO_4$	5.96	5.62	2.95
(7)	$[Mn_2L^3]ClO_4$	5.59	4.00	1.59

Table 8. Magnetic susceptibility parameters

	Compound	J/cm^{-1}	g
(1)	$[Mn_2L^1Cl_2]$	0.20*	2.11*
(2)	$[Mn_2L^2Cl_2]$	0.30	1.98
(3)	$[Mn_2L^1Br_2]$	0.11	2.05
(4)	$[Mn_2L^2Br_2]$	0.18	2.09
(5)	$[Mn_2L^1(MeCO_2)]ClO_4$	−0.82	1.94
(6)	$[Mn_2L^2(MeCO_2)]ClO_4$	−0.79	2.00

* Ref. 6.

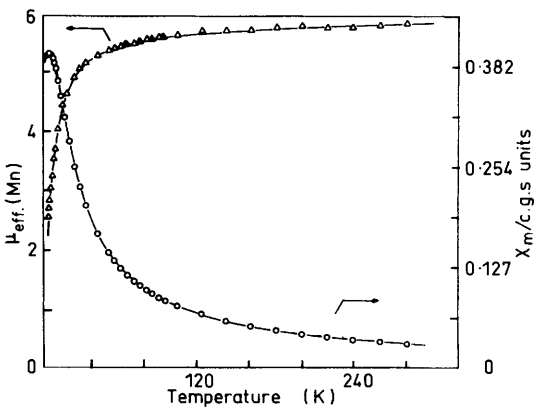

Figure 8. Variable-temperature magnetic susceptibility data for $[Mn_2L^1(MeCO_2)]ClO_4$ (**5**). The solid lines result from a least-squares fit of the data to the theoretical equation for isotropic magnetic exchange in a binuclear unit with $S_1 = S_2 = \frac{5}{2}$

acetate anions to afford the infinite chains. I.r. spectroscopy and the *X*-ray powder diffraction pattern indicate that (**5**) includes, most likely, binuclear units similarly bridged by acetate anions to afford chains (**6**). On the other hand, the *X*-ray powder diffraction patterns of (**1**)—(**4**) indicate that all four complexes are isostructural with $[Co_2L^1Br_2]$ which has independent binuclear units. This led us, for comparison purposes, to fit the magnetic susceptibility data for complexes (**2**)—(**6**) to the theoretical susceptibility equation resulting from consideration of isotropic intramolecular exchange interaction (J), with the inclusion of intermolecular exchange ($Z'J'$) in the molecular field approximation.[34] Single-ion zero-field interactions DS_z^2 were not taken into account in our theoretical susceptibility equation in order to avoid overparameterization. Actually, Ginsberg *et al.*[34b] have shown that the parameters D and $Z'J'$ are very strongly correlated. The intermolecular exchange parameters resulting from these fits are at least one order of magnitude smaller than the intra-dimer exchange parameter J (with $0.1 < |J| < 1$ cm^{-1}). This leads to the conclusion that the intermolecular exchange interaction is negligible in complexes (**2**)—(**6**). Consequently, the data were also least-squares fitted to the theoretical equation[9] for an isotropic magnetic exchange

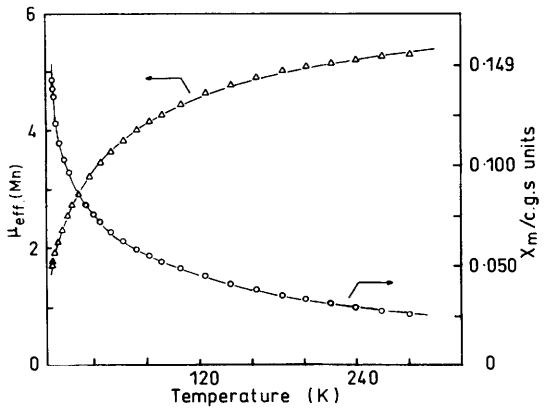

Figure 9. Variable-temperature magnetic susceptibility data for $[Mn_2L^3]ClO_4$ (**7**). The solid lines result from a least-squares fit of the data to the theoretical equation for isotropic magnetic exchange in a binuclear unit with $S_1 = S_2 = \frac{5}{2}$ and with the inclusion of intermolecular exchange ($Z'J'$)

between two, $S_1 = S_2 = \frac{5}{2}$, ions by employing the simpler spin Hamiltonian $\mathcal{H} = -2JS_1.S_2$. The solid lines in Figures 7 and 8 represent those fits which can be seen to be good. The parameters J and g obtained from these fits are summarized in Table 8.

The complex $[Mn_2L^3]ClO_4$ (**7**) has an effective magnetic moment [$\mu_{eff.}$(Mn) = 5.6] which is lower than the spin-only value at room temperature. The decrease in effective magnetic moment with decreasing temperature is regular over the whole temperature range and results in the lowest effective magnetic moment (1.6) observed at 5 K in this series (Figure 9). It was impossible to obtain a reasonable fit for this complex by employing the simple spin Hamiltonian $\mathcal{H} = -2JS_1.S_2$. The theoretical susceptibility equation resulting from consideration of both the isotropic intra-dimer exchange interaction (J) and inter-dimer exchange interaction ($Z'J'$) in the molecular field approximation[34] affords a reasonable fit (Figure 9). The parameters obtained from that fit are: $J = -0.3$ cm^{-1}, $J' = -5.2$ cm^{-1}, and $g = 1.93$. Even though the much larger inter-dimer exchange interaction compared to the intra-dimer one indicates that the theoretical susceptibility equation derived by Ginsberg and Lines[34a] is not suitable in the case of complex (**7**), these results show the presence of more than one type of antiferromagnetic exchange interaction in this complex. However, one must await precise structural information on complex (**7**) in order to know if the variation in the effective magnetic moment with temperature results from the presence of two or more different intramolecular antiferromagnetic exchange interactions in a $([Mn_2L^3]ClO_4)_2$ tetranuclear complex, as evidenced by Kolks and Lippard[35] for $[Cu_2(bpim)(im)]_2[NO_3]_4$ {bpim = 4,5-bis[2-(2-pyridyl)ethyliminomethyl]-imidazolate, im = imidazolate}.

The variable-temperature magnetic susceptibility studies confirm that complexes (**1**)—(**7**) include three different structural species. The four complexes incorporating co-ordinating halide anions have manganese(II) ions displaced in opposite directions from the L^1 or L^2 ligand plane. This results in a reduction of the effectiveness of the dominant antiferromagnetic exchange pathway consisting of two $d_{x^2-y^2}$ orbitals, one on each manganese(II) ion, interacting *via* the *s* and *p* orbitals of the phenolate oxygen atoms. In addition, there are five electrons per metal ion, which brings about ferromagnetic exchange pathways and leads to a net ferromagnetic interaction for these four complexes. The low and similar values of the exchange parameters of (**1**)—(**4**) allow the conclusion that the secondary alcoholic function present in complexes (**2**) and (**4**) does not appreciably modify the exchange interaction, indicating that the alcoholic oxygen is not co-ordinated either intra- or intermolecularly to a manganese ion.

In complex (**6**), the manganese(II) ions of a binuclear unit are bridged by two phenolate oxygen atoms and their distance is 3.27 Å, while the distance between two manganese ions bridged by an acetato group in a chain of binuclear units is 6.22 Å (*cf.* molecular structure discussed earlier). We have already shown in this paper that even for complexes (**5**) and (**6**) the intermolecular exchange interactions are at least one order of magnitude smaller than the intramolecular ones. Thus, as expected, the two phenolate oxygen bridges mediate manganese–manganese magnetic exchange interactions more efficiently than do the acetato groups. Hence, the net antiferromagnetic exchange interaction observed for complexes (**5**) and (**6**) results from the relative positions of the two manganese ions in a binuclear unit. For both complexes, the co-ordinating halide anions have been replaced by a non-co-ordinating perchlorate and a bridging acetate anion. Both modifications allow a smaller departure of the manganese ions from the macrocyclic ligand plane. In particular, the negative charge of an acetate anion can be viewed as equally shared by both oxygen atoms of the acetate. This, together with the fact that oxygen atoms are smaller than chloride or bromide anions, allows the manganese(II) ions to stay closer to the macrocyclic ligand plane in complexes (**5**) and (**6**) compared to (**1**)—(**4**). This results in an increase in the effectiveness of the antiferromagnetic exchange pathways and affords the first examples of manganese(II) complexes with Robson-type ligands characterized by a predominance of the antiferromagnetic exchange pathways over the ferromagnetic ones.

In complex (**7**) where the alcoholic oxygen of the L^2 ligand is deprotonated and acts as a bridging anion the predominance of the antiferromagnetic exchange pathways is further increased. As shown from the large angle *X*-ray scattering study of (**7**), the most plausible structural hypothesis is to consider that two $Mn_2L^3(ClO_4)$ units are bridged by the two alcoholate oxygen atoms to afford a tetranuclear structure, as represented in Figure 2(*c*). This presumed structural arrangement would afford the possibility of a second antiferromagnetic exchange interaction between the manganese ions of the two intervening binuclear units of a tetranuclear complex. We are pursuing efforts to grow crystals of this new polynuclear complex.

E.S.R. Spectroscopy.—Complexes $[Mn_2L^1Cl_2]$·MeOH (**1**) and $[Mn_2L^2Cl_2]$·MeOH (**2**) exhibit *X*-band powder e.s.r. spectra (4, 100, and 300 K) (see SUP 56703) characterized by two broad resonances centred near $g_{eff.} \approx 6$ (greatest intensity resonance) and $g_{eff.} \approx 2$. Due to the insolubility of these complexes in the usual solvents, it was not possible to obtain solution or glass e.s.r. spectra. Similar powder e.s.r. spectra have been previously observed for axially distorted and for trigonal-bipyramidal mononuclear manganese(II) complexes.[2,36,37] The *X*-band powder e.s.r. spectra of (**1**) and (**2**) which are characteristic of near-axial symmetry are in agreement with the structural features previously discussed, *i.e.* square pyramidal or pseudo-square-pyramidal geometry around each manganese(II) ion.

The zero-field splitting parameters estimated by using the theoretical approach of Dowsing *et al.*[36a] are $D \approx 0.1$ cm^{-1} and $\lambda (= E/D) < 0.1$ (D and E are the axial and rhombic zero-field splitting parameters, respectively). The similarity of the fine-structure patterns of (**1**) and (**2**) with those described for electronically isolated manganese species[2,36,37] indicates that the small ferromagnetic interactions operating between the two manganese(II) ions of a binuclear unit do not modify appreciably the e.s.r. spectra of these complexes, even at very

low temperature. The *Q*-band powder e.s.r. spectra (120 and 300 K) of (**1**) and (**2**), characterized by several broad resonances, occurring between 0 and 14 500 G, are similar to those previously observed for electronically isolated manganese(II) species[37,*] and further substantiate the interpretation of the *X*-band powder spectra.

Complexes $[Mn_2L^1Br_2]$·MeOH (**3**) and $[Mn_2L^2Br_2]$·MeOH (**4**) exhibit *X*-band powder e.s.r. spectra (4, 110, and 300 K) characterized by several broad resonances, spread between 500 and 7 000 G, with the greatest intensity resonance at *ca.* 500 G. The 300 K spectra exhibit a very important broadening of the lines to a point where the signal-to-noise ratio is very small. The *Q*-band e.s.r. spectra (120 and 300 K) of (**3**) and (**4**) are also characterized by several resonances spread out from 500 to 14 000 G with the greatest intensity resonance at *ca.* 5 000 G. To our knowledge, similar *X*-band and *Q*-band spectra have not been previously reported. The observation of resonances at very low field values indicates that the zero-field splitting between two Kramers doublets is of the order of magnitude of $h\nu$.

Taking into account the results of both the magnetic susceptibility and e.s.r. measurements for complexes (**1**)—(**4**) leads us to consider that the ferromagnetic interaction ($0.1 < J < 0.3$ cm^{-1}) is larger than the zero-field splitting parameter D (≈ 0.1 cm^{-1}) for the complexes containing chloride anions [(**1**) and (**2**)] while the situation seems to be reversed for the complexes containing bromide anions [(**3**) and (**4**)]. As for complexes (**1**) and (**2**), it seems that the powder e.s.r. spectra of (**3**) and (**4**) are not noticeably influenced by the small ferromagnetic interaction operating between the two manganese(II) ions of a binuclear unit.

Finally the observed differences in the *X*-ray powder diffraction spectra of complexes (**1**) and (**2**), compared with complexes (**3**) and (**4**) (*cf.* *X*-ray powder diffraction spectra section), can be related to the difference in distortion leading to the e.s.r. and magnetic susceptibility results discussed here.

Complexes $[Mn_2L^1(MeCO_2)]ClO_4$·MeOH (**5**) and $[Mn_2L^2(MeCO_2)]ClO_4$·MeOH (**6**) exhibit *X*-band powder e.s.r. spectra (4, 110, and 300 K) characterized by a very broad ($\approx$ 2 000 G, peak to peak) isotropic resonance with $g_{eff.}$ values of *ca.* 1.95. The *Q*-band powder e.s.r. spectra obtained at 120 and 300 K have similar characteristics. Such e.s.r. spectra have been shown to arise from associated polynuclear species.[2,36a,38] The *X*-band frozen solution e.s.r. spectra of (**5**) and (**6**) obtained from dmf–toluene glasses at 4 and 110 K are very similar and exhibit 15 fine-structure resonances spread over 0 to 9 000 G. Several of these resonances are further split into an 11-line pattern with relative intensities close to the ratio, 1:2:3:4:5:6:5:4:3:2:1. The hyperfine coupling constant for these patterns is 44 ± 2 G. The *Q*-band frozen solution e.s.r. spectra do not afford such nicely resolved patterns. However, fine-structure transitions ranging from 8 000 to 14 000 G may still be easily discerned. As recently discussed in detail for [Mn^{II}(saldien)][saldien = 3-azapentane-1,5-diylbis(salicylideneiminate)][2] and as previously shown by several authors,[39] the hyperfine intensity pattern and magnitude of coupling constant clearly indicate that, in frozen solution, these complexes include pairs of interacting manganese(II) ions. These results are in agreement with the interpretation of the magnetic susceptibility data as arising from a weak (*ca.* -0.8 cm^{-1}) intramolecular antiferromagnetic exchange interaction between two manganese(II) ions in (**5**) and (**6**).

The observation of a very broad isotropic e.s.r. resonance in the solid state for both complexes is in agreement with the results of the *X*-ray structural determination of (**6**). The binuclear units are not isolated but bridged by acetato groups into infinite chains. Intermolecular interactions transmitted through the acetato groups of an infinite chain, even if they are too small to be detected by magnetic susceptibility measurements, can constitute an effective pathway for spin–spin exchange broadening in the solid state. In the dmf–toluene glasses, the dissolution and resulting magnetic dilution affords magnetically isolated binuclear species exhibiting only the isotropic antiferromagnetic interactions of a pair of similar exchange coupled manganese(II) ions.

$[Mn_2L^3]ClO_4$ (**7**) exhibits *X*-band powder e.s.r. spectra (4, 110, and 300 K) characterized by a very broad resonance centred near $g_{eff.} = 2$. The *Q*-band powder e.s.r. spectra (120 and 300 K) are similarly characterized by $g \approx 2$ centred broad resonance. The *X*-band frozen solution e.s.r. spectra obtained from dmf–toluene glasses are similar at 4 and 110 K and exhibit several fine-structure resonances spread from 0 to 7 000 G. The resolution of these resonances is enhanced on the 4 K compared to the 110 K spectrum but the overall appearance of both spectra is related to that of the 4 K powder spectrum. However, two fine-structure resonances are further split into the characteristic 11-line pattern with a hyperfine coupling constant of 43 ± 2 G. As already observed for [Mn(saldien)][2] and for complexes (**5**) and (**6**) (see above), the *Q*-band glass e.s.r. spectrum, although not as well resolved as the *X*-band glass spectra, show a fine-structure pattern including several resonances spread from 8 000 to 14 000 G.

As previously stated for (**5**) and (**6**), the broad resonance observed at *X*- and *Q*-band for powdered samples of (**7**) is different from the spectrum of an isolated binuclear species and characteristic of the presence of more than one type of magnetic exchange interaction. The main differences between (**7**) and (**5**) [or (**6**)] are observed in the *X*- and *Q*-band glass spectra that are poorly resolved for (**7**) compared to (**5**) or (**6**). The experimental conditions being identical, the magnetic dilution of (**7**) must be similar to that of (**5**) or (**6**). The relative intensities of the eleven lines of the hyperfine pattern and the magnitude of *A* clearly indicating that (**7**) includes pairs of interacting manganese(II) ions, it is thus clear that the differences in the glass spectra of (**7**) and (**5**) [or (**6**)] originate in the nature of the other magnetic exchange interactions operating in (**7**). This may be explained as follows. In (**5**) and (**6**), the magnetic exchange interaction superimposed on the isotropic antiferromagnetic interaction operating inside the binuclear units is mediated by the acetate bridges affording infinite chains. In solution, the coordinating solvent molecules break down the chains and afford magnetically isolated binuclear species characterized by the glass e.s.r. spectra described for (**5**) and (**6**). For complex (**7**) and taking into account the structural hypothesis described (see large angle *X*-ray scattering section), the magnetic exchange interactions superimposed on the isotropic antiferromagnetic interaction operating inside the binuclear units should be mediated by the alcoholate anions bridging two binuclear units and pertaining to the macrocyclic ligands. Thus, these interactions are localized and operate inside each tetranuclear species. The solvation of (**7**) by the dmf–toluene solvent mixture may result in a magnetically diluted medium including non-dissociated tetranuclear species as well as dissociated binuclear units. Such a situation would account for the observed glass e.s.r. spectra as resulting from the superimposition of the spectra of magnetically isolated binuclear and tetranuclear species.

Conclusions

The seven manganese(II) complexes described in this study include Robson-type macrocyclic ligands affording an identical in-plane N_4O_2 donor set to a pair of manganese(II) ions.

* Very similar *Q*-band powder e.s.r. spectra have been obtained in this laboratory for the complex [4-azaheptane-1,7-diylbis(salicylideneiminato)]manganese(II), and the 5,5′-dinitro ring-substituted derivative, described in ref. 2.

However, the i.r., e.s.r., variable-temperature magnetic susceptibility, and *X*-ray structural studies show that the chemical nature and co-ordination ability of the associated anions induce three types of molecular structures for these complexes, including isolated binuclear units, (**1**)—(**4**), infinite chains of binuclear units bridged by acetate anions, (**5**) and (**6**), or tetranuclear species, (**7**). It should be noted that while the deprotonation of the acoholic function of (**6**) leads to (**7**) the deprotonation of (**2**) and (**4**) does not result in the formation of new complexes similar to (**7**). This observation confirms that the chloride or bromide anions are strongly co-ordinated to the manganese ions of (**2**) and (**4**) respectively while the bridging acetate anions of (**6**) are easily displaced either by co-ordinating solvent molecules (*cf.* e.s.r. spectroscopy section) or the alcoholate oxygen of the L^3 ligand.

Compounds (**5**), (**6**), and (**7**) are the first manganese(II) complexes with Robson-type ligands exhibiting antiferromagnetic exchange interactions. Their magnetic behaviour is similar to that recently described for two manganese(II) binuclear complexes with metal centres bridged by three oxygen atoms.[40] The information presently available on (**7**) indicates that it is the first manganese tetranuclear complex with a geometry different from the cubane[41] or adamantane[42] ones already reported for tetranuclear manganese complexes. Finally, complex (**7**) exhibits the strongest antiferromagnetic interactions already reported for a polynuclear manganese(II) complex.

Acknowledgements

We thank the Etablissement Public Régional and the Action de Recherche Intégrée 'Chimie-Biologie' for partial support of this work.

References

1 B. Mabad, J-P. Tuchagues, Y. T. Hwang, and D. N. Hendrickson, *J. Am. Chem. Soc.*, 1985, **107**, 2801.
2 B. Mabad, P. Cassoux, J-P. Tuchagues, and D. N. Hendrickson, *Inorg. Chem.*, 1986, **25**, 1420.
3 N. H. Pilkington and R. Robson, *Aust. J. Chem.*, 1970, **23**, 2225.
4 B. F. Hoskins and G. A. Williams, *Aust. J. Chem.*, 1975, **28**, 2607.
5 B. F. Hoskins, N. J. McLeod, and H. A. Schaap, *Aust. J. Chem.*, 1976, **29**, 515.
6 S. L. Lambert and D. N. Hendrickson, *Inorg. Chem.*, 1979, **18**, 2683.
7 R. R. Gagné, C. L. Spiro, T. J. Smith, C. A. Hamann, W. R. Thies, and A. K. Shiemke, *J. Am. Chem. Soc.*, 1981, **103**, 4073.
8 S. L. Lambert, C. L. Spiro, R. R. Gagné, and D. N. Hendrickson, *Inorg. Chem.*, 1982, **21**, 68.
9 C. L. Spiro, S. L. Lambert, T. J. Smith, E. N. Duesler, R. R. Gagné, and D. N. Hendrickson, *Inorg. Chem.*, 1981, **20**, 1229.
10 B. F. Hoskins, R. R. Robson, and G. A. Williams, *Inorg. Chim. Acta*, 1976, **16**, 121.
11 (*a*) R. R. Gagné, C. A. Koval, and J. A. Smith, *J. Am. Chem. Soc.*, 1977, **99**, 8367; (*b*) R. R. Gagné, C. A. Koval, J. A. Smith, and M. C. Cimolino, *ibid.*, 1979, **101**, 4571; (*c*) R. R. Gagné, L. M. Henling, and T. J. Kistenmacher, *Inorg. Chem.*, 1980, **19**, 1226.
12 R. C. Long and D. N. Hendrickson, *J. Am. Chem. Soc.*, 1983, **105**, 1513.
13 J. C. De Paula and G. W. Brudvig, *J. Am. Chem. Soc.*, 1985, **107**, 2643; T. Kambara and Govindjee, *Proc. Natl. Acad. Sci. USA*, 1985, **82**, 6119; J. C. De Paula, W. F. Beck, and G. W. Brudvig, *J. Am. Chem. Soc.*, 1986, **108**, 4002; G. Renger and Govindjee, *Photosynth. Research*, 1985, **6**, 33; Govindjee, T. Kambara, and W. Coleman, *Photochem. Photobiol.*, 1985, **42**, 187; T. Kambara, S. Padhye, D. N. Hendrickson, and Govindjee, *Photosynth. Research*, 1986, **9**, 103.
14 F. Ullman and K. Brittner, *Chem. Ber.*, 1909, **42**, 2539.
15 J. P. Chandler, Quantum Chemistry Program Exchange, Indiana University, Program 66.
16 A. Mosset, J-J. Bonnet, and J. Galy, *Acta Crystallogr., Sect. B*, 1977, **33**, 2639.
17 B. A. Frentz, SDP-Structure Determination Package, Enraf-Nonius, Delft, 1982.
18 P. Main, S. E. Hull, L. Lessinger, G. Germain, J. P. Declercq, and M. H. Woolfson, MULTAN 80, Universities of York and Louvain, Belgium, 1980.
19 W. D. Carlisle, D. E. Fenton, P. B. Roberts, U. Casellato, P. A. Vigato, and R. Graziani, *Transition Met. Chem.*, 1986, **11**, 292.
20 V. McKee and J. Smith, *J. Chem. Soc., Chem. Commun.*, 1983, 1465.
21 D. T. Cromer and J. T. Waber, in 'International Tables for *X*-Ray Crystallography,' eds. J. A. Ibers and W. C. Hamilton, Kynoch Press, Birmingham, 1974, vol. 4, Table 2.2.B, pp. 99—101.
22 D. T. Cromer, in ref. 21, Table 2.3.1, p. 149.
23 G. M. Sheldrick, SHELX 76, Program for Crystal Structure Determination, University of Cambridge, 1976.
24 C. K. Johnson, ORTEP, Report ORNL-3794, Oak Ridge National Laboratory, Oak Ridge, Tennessee, 1965.
25 J. Galy, A. Mosset, and P. Lecante, F.P. 80.16170/1980; U.K.P. 2081440B/1984, U.S.P. 4 475 225/1985.
26 P. Lecante, A. Mosset, and J. Galy, *J. Appl. Crystallogr.*, 1985, **18**, 214.
27 J. Krogh-Moe, *Acta Crystallogr.*, 1956, **9**, 951; A. Burian, B. Rzepa, P. Lecante, and A. Mosset, *J. Mater. Sci. Lett.*, 1985, **4**, 701.
28 D. T. Cromer, *J. Chem. Phys.*, 1969, **50**, 4857.
29 F. Zernicke and J. A. Prins, *Z. Phys.*, 1927, **41**, 184—187.
30 P. Debye, *Ann. Phys. (Leipzig)*, 1915, **46**, 809.
31 G. B. Deacon and R. J. Phillips, *Coord. Chem. Rev.*, 1980, 33, 227.
32 K. Yvon, W. Jeitschko, and E. Parthe, LAZY PULVERIX program, University of Geneva, Switzerland, 1977.
33 L. Ericsson and M. Westdahl, TREOR program, *J. Appl. Crystallogr.*, 1985, **18**, 367.
34 (*a*) A. P. Ginsberg and M. E. Lines, *Inorg. Chem.*, 1972, **11**, 2289; (*b*) A. P. Ginsberg, R. L. Martin, R. W. Brookes, and R. C. Sherwood, *ibid.*, p. 2884.
35 G. Kolks and S. J. Lippard, *J. Am. Chem. Soc.*, 1977, **99**, 5804.
36 (*a*) R. D. Dowsing, J. F. Gibson, M. Goodgame, and P. J. Hayward, *J. Chem. Soc. A*, 1969, 187; *ibid.*, 1969, 1242; (*b*) D. M. Goodgame, M. Goodgame, and P. J. Hayward, *ibid.*, 1970, 1352.
37 E. J. Laskowski and D. N. Hendrickson, *Inorg. Chem.*, 1978, **17**, 457—470.
38 R. D. Dowsing, J. F. Gibson, D. M. Goodgame, M. Goodgame, and P. J. Hayward, *Nature (London)*, 1968, **219**, 1037.
39 B. A. Coles, J. W. Orton, and J. Owen, *Phys. Rev. Lett.*, 1960, **4**, 116; A. Hudson and M. J. de G. Kennedy, *Inorg. Nucl. Chem. Lett.*, 1971, **7**, 333; R. J. Van Zee, C. A. Baumann, and W. Weltner, jun., *J. Chem. Phys.*, 1981, **74**, 6977; C. A. Baumann, R. J. Van Zee, S. V. Bhat, and W. Weltner, jun., *ibid.*, 1983, **78**, 190; P. Mathur and G. C. Dismukes, *J. Am. Chem. Soc.*, 1984, **106**, 2041.
40 M. D. Timken, W. A. Marritt, D. N. Hendrickson, R. A. Gagné, and E. Sinn, *Inorg. Chem.*, 1985, **24**, 4202.
41 V. McKee and W. B. Shepard, *J. Chem. Soc., Chem. Commun.*, 1985, 158.
42 K. Wieghardt, U. Bossek, and W. Gebert, *Angew. Chem., Int. Ed. Engl.*, 1983, **22**, 328.

Received 5th March 1987; *Paper* 7/414